Iranian Journal of Oil & Gas Science and Technology, Vol. 8 (2019), No. 4, pp. 85-105
http://ijogst.put.ac.ir

Prediction of Dispersed Phase Holdup in the Kühni Extraction Column Using a New Experimental Correlation and Artificial Neural Network

Mohsen Keshavarz[1], Ahad Ghaemi[2*], Mansour Shirvani[3], and Ebrahim Arab[4]

[1] M.S. Student, School of Chemical, Petroleum, and Gas Engineering, Iran University of Science and Technology, P.O. Box 16846-13114, Tehran, Iran
[2] Associate Professor, School of Chemical Engineering, Iran University of Science and Technology, P.O. Box 16846-13114, Tehran, Iran
[3] Associate Professor , School of Chemical Engineering, Iran University of Science and Technology, P.O. Box 16846-13114, Tehran, Iran
[4] M.S. Student, School of Chemical Engineering, Iran University of Science and Technology, P.O. Box 16846-13114, Tehran, Iran

Received: August 13, 2018; *revised*: November 08, 2018; *accepted*: December 19, 2018

Abstract

In this work, the dispersed phase holdup in a Kühni extraction column is predicted using intelligent methods and a new empirical correlation. Intelligent techniques, including multilayer perceptron and radial basis functions network are used in the prediction of the dispersed phase holdup. To design the network structure and train and test the networks, 174 sets of experimental data are used. The effects of rotor speed and the flow rates of the dispersed and continuous phases on the dispersed phase holdup are experimentally investigated, and then the artificial neural networks are designed. Performance evaluation criteria consisting of R^2, RMSE, and AARE are used for the models. The RBF method with R^2, RMSE, and AARE respectively equal to 0.9992, 0.0012, and 0.9795 is the best model. The results show that the RBF method well matches the experimental data with the lowest absolute percentage error (2.1917%). The rotor speed has the most significant effect on the dispersed phase holdup comparing to the flow rates of the continuous and dispersed phases.

Keywords: Solvent Extraction, Kühni Extraction Column, Dispersed Phase Holdup, Multilayer Perceptron, Radial Basis Function.

1. Introduction

Liquid-liquid extraction is an important separation process used in many industries such as petroleum, petrochemical, pharmaceutical, food, environmental, nuclear, and hydrometallurgical industries (Arab et al., 2017; Oliveira et al., 2008; Moreira et al. 2005). Various types of solvent extraction contactors have been used in liquid-liquid extraction processes (Hemmati et al., 2015; Torab-Mostaedi et al., 2011). There are two common types of phase agitation: by rotary agitation by discs, turbines, etc., and by pulsations. Among the wide variety of equipment, a counter-current column with a rotary agitator is more frequently utilized (Asadollahzadeh et al., 2015a, 2015b; Hemmati et al., 2015; Haunold et al.,

* Corresponding author:
Email: aghaemi@iust.ac.ir

1990). The Kühni column is one of the most important agitation column extractors. It includes a rotating shaft inside the column on which a number of impellers are mounted and separated by perforated static horizontal plates to make a number of agitation stages (Mogli and Buhlmann, 1983; Tahershamsi et al., 2016). The design and identification of the performance of liquid-liquid extraction columns for achieving the effects of operating variables at scaling-up stages require the careful consideration of the hydrodynamic and mass transfer parameters of the device. In a liquid-liquid extraction column, the dispersed phase droplets undergo repeated coalescence and breakage, ultimately causing an equilibrium drop size distribution. The resulting fractional volumetric holdup of the dispersed phase is defined as the volume fraction of the active section of the column that is occupied by the dispersed phase (Torab-Mostaedi et al., 2011):

$$\phi = \frac{V_d}{\left(V_C + V_d\right)} \tag{1}$$

The dispersed phase holdup is one of the most important hydrodynamic parameters in extraction columns since it affects both the flooding specification and the mass transfer characteristic of the column. Also, the dispersed phase holdup is used to calculate the interfacial area and the residence time of droplets (Kumar and Hatland, 1995). The dispersed phase holdup is necessary for calculating the slip velocity between the phases in extraction columns. There are two methods for calculating the dispersed phase holdup, including explicit and implicit methods. In the implicit method, the slip velocity is used to achieve the dispersed phase holdup. The available proposed correlations are either approximate or usable in a specified range of operation conditions. There are a lot of experimental studies performed on various scales of the Kühni extraction column to determine the hydrodynamic and mass transfer parameters of the column. Kumar et al. (1986) investigated the change of the dispersed phase holdup and flooding point for a water-ortho-xylene system in the Kühni extraction column. They understood that the variations of the dispersed phase holdup along the column was not uniform and that the effects of the speed of rotation and the flow rates of the continuous (Q_c) and dispersed (Q_d) phases on the dispersed phase holdup were almost similar, while the maximum of the dispersed phase holdup occurred almost in the middle stages of the column. Hufnagl et al. (1991) provided a differential model for mass transfer from the continues to the dispersed phase in a toluene-acetone-water system in the Kühni extraction column (Hufnagl et al., 1991). Oliveira et al. (2008) evaluated the effects of operational parameters on the dispersed phase holdup for a water-Exxsol D-80 system (Oliveria et al., 2008). Florian et al. (2012) studied the separation of toluene from heptane. They used population balance modeling to simulate a pilot-scale Kühni extraction column (Florian et al., 2012). Arthur and Mansur (2013) used a combination of a dynamic model with the droplet population balance equations to simulate the Kühni extraction column (Neto and Mansur, 2013). Some of the correlations proposed for predicting the dispersed phase holdup in different types of extractor columns are summarized in Table 1.

Mechanical mixing devices or pulsing mechanisms are used for agitation in the liquid-liquid extraction columns to improve mass transfer rate, which increases the complexity of the process modeling in such columns (Florian et al., 2012). The modeling and simulation of the extraction devices are necessary for determining the affecting parameters and their impact on the performance of equipment. The model of the process involves a wide set of equations, and solving them simultaneously is difficult and time-consuming (Gomes et al., 2006; Rode et al., 2013; Attarakih et al., 2015). On the other hand, the numerical methods of artificial neural networks (ANN) have found a wide interest in the modeling of process systems in recent years.

Table 1

Summary of correlations for the calculation of the dispersed phase holdup in different contactors.

Type of column	Correlation	Reference
RDC	$\phi = 1.37\exp\left(0.59\frac{N^2D}{g}\right)\left(\frac{V_d}{Dg}\right)^{0.42}\left(1+\frac{V_c}{V_d}\right)^{0.26}\left(\frac{\mu_c}{\sqrt{\gamma\rho_c D}}\right)^{0.12}\left(\frac{D^2\rho_c g}{\gamma}\right)^{0.15}\left(\frac{\Delta\rho}{\rho_c}\right)^{-0.56}\left(\frac{h_c}{D}\right)^{-1.18}$	Haunold et al., 1990
RDC	$\phi = k\left(\frac{D_s}{D}\right)^{-2.1}\left(\frac{h_c}{D}\right)^{-0.75}\left(\frac{D}{T}\right)^{-2.5}\left[\left(\frac{g}{DN^2}\right)^{-0.33}\left(\frac{\gamma^3\Delta\rho}{\mu_c^4 g}\right)^{-0.07}\left(\frac{\Delta\rho}{\rho_c}\right)^{-0.2}\right]^n\left[\frac{V_d}{\left(\frac{\gamma\Delta\rho g}{\rho_c^2}\right)^{0.25}}\right]\left(1+\frac{V_c}{V_d}\right)^{0.15}$	Torab-Mostaedi et al., 2011
Kühni	$\phi = 2.76\times10^{-2}+\left[\frac{\psi}{g}\left(\frac{\rho_c}{g\gamma}\right)^{0.25}\right]^{0.77}\left[V_d\left(\frac{\rho_c}{g\gamma}\right)^{0.25}\right]^{0.64}\exp\left[20.7\times V_c\left(\frac{\rho_c}{g\gamma}\right)^{0.25}\right]0.56\left(\frac{\Delta\rho}{\rho_c}\right)^{-0.34}\left(2.27\times e^{-0.77}\right)$	Haunold et al., 1990
Kühni	$\phi = (0.6\pm0.2)Q_d^{0.8\pm0.2}N_R^{1.6\pm0.3}$	Oliveira et al., 2088
ORC	$\phi = 0.1728+0.4406V_d+0.1158h+0.0247N$	Sharker et al., 1985

In this work, two different methods of ANN are used to predict the dispersed phase holdup of the Kühni extraction column. The data are from the two liquid-liquid systems, namely toluene-water and n-butyl acetate-water systems, with different physical properties in the condition of no mass transfer. The experiments were conducted to determine the effects of operating parameters such as the rotor speed and the flow rates of the continuous and dispersed phases on the dispersed phase holdup. A set of 174 experimental data were used in the artificial neural networks, from which 93 data were from toluene-water system and 81 data from n-butyl acetate-water system. The inputs were the speed of rotation and the flow rates of the dispersed and continuous phases, and the output was the dispersed phase holdup.

The purpose of the current paper is to develop artificial intelligence-based models for predicting the dispersed phase holdup in the Kühni extraction column. The comparison of the ability of empirical correlation and ANN models to predict anonymous data can be considered as the innovation of this paper. Due to the complexity of the design of extraction columns and the effects of multiple parameters, using ANNs-based artificial intelligence can obviate the need for experimental data to some extent by reducing the cost of the experiments.

2. Experimental

There are numerous methods such as local displacement, pressure drops, and sampling methods for measuring the dispersed phase holdup in the extraction columns (Chen et al., 2002). The experiments were carried out using a pilot-scale Kühni extraction column. The active portion of the column was

made of a transparent plastic material resistant to the solvent used in the experiments (Arab et al., 2017). The column consisted of 10 stages, each stage being separated by the perforated plates, each of which includes 36 holes with a diameter of 5.7 mm (Figure 1). The aqueous phase is introduced at the top of the column flowing downward, and the dispersed phase flows counter-currently. Agitation at each stage is achieved with a six-blade turbine agitator having a diameter of 50 mm with accurate speed control. In all the experiments, water is used as the continuous phase and the organic solvent as the dispersed phase. All the experiments were carried out far from flooding conditions. All the physical properties of the liquid systems reported in Table 2 are constant.

Table 2

Physical properties of the tested systems (Arab et al., 2017).

Physical property	Toluene-water	n-Butyl acetate-water
$\rho_c\left(\frac{Kg}{m^3}\right)$	998.2	997.8
$\rho_d\left(\frac{Kg}{m^3}\right)$	865.2	882.3
$\mu_c\left(mPa.s\right)$	0.96	1.04
$\mu_d\left(mPa.s\right)$	0.75	0.76
$\gamma\left(\frac{mN}{m}\right)$	36.10	14.10

Two PENTAX centrifugal pumps were used to move the light and heavy phase. A 1.1 kW electric motor (MOTOGEN Company, Iran) was used to rotate the extraction column. An optical sensor was used to control the interface between two phases at the top of the column. Four metal tanks made of stainless steel with a volume of about 85 liters were built to hold and collect the light and heavy phases. Duo to the experimental limits, in these experiments the ratio of the mixer diameter to the column diameter is constant (Arab et al., 2017).

Figure 1

A schematic of the Kühni extraction column (Arab et al., 2017).

The liquid systems studied are toluene–water and n-butyl acetate–water. These systems have been recommended by the European Federation of Chemical Engineering (EFCE) as official test systems for extraction investigations. During the experiments, the effects of rotor speed and the flow rates of the dispersed and continuous phases on the dispersed phase holdup were studied. A rotor speed in the range of 90 to 270 rpm and the flow rates of the dispersed and continuous phases in the range of 18 to 42 lit/hr. were applied. In each experiment, one of the parameters was changed while the others were kept constant. Totally, 93 data sets of toluene-water and 81 data sets of n-butyl acetate-water were obtained and used in the modeling procedures. The range of the inputs and the details of the information on the simulation are tabulated in Table 3 (Arab et al., 2017).

Table 3

Details of the collected information on both systems used in the experiments.

System	Inputs parameter	Ranges	The mean of the parameter	Standard deviation
Toluene-water	Rotor speed (rpm)	90-270	154.1940	46.0404
	Flow rate of the dispersed phase, Q_d (l/hr.)	18-42	26.9355	6.1996
	Flow rate of the continuous phase, Q_c (l/hr.)	18-42	26.9355	6.1996
n-Butyl acetate-water	Rotor speed (rpm)	90-210	144.0740	39.6640
	Flow rate of the dispersed phase, Q_d (l/hr.)	18-40	26.4200	4.8190
	Flow rate of the continuous phase, Q_c (l/hr.)	20-36	25.7780	4.0000

3. Artificial intelligence-based models

Various methods of ANN's can be considered as a class of dynamical systems that process and develop a model from the experimental data and the knowledge or law behind the data (Du et al., 2006). They are computational tools which can be considered as computational intelligence. The origin of the method is taken from the principles of biology arranged in a mathematical description by scientists. One of the key ideas in artificial neural networks is the back-propagation algorithm created by David Rummelhart and James McClelland in 1986. The back-propagation algorithm is a common method for training AANs, which is used to minimize the cost function. The back-propagation algorithm is a supervisory learning method which requires a set of input-output data (Hassoun et al., 1996).

The multi-layer perceptron (MLP) is one of the most famous artificial neural networks used to create non-linear mappings. It is a kind of feed-forward artificial neural network which is able to perform a non-linear mapping with arbitrary precision by selecting the number of layers and neurons. The adjustable parameters of the network are the weights of the connections between the layers. The MLP network consists of three layers: the input layer, the hidden layer, and the output layer (Hagan and Menhaj, 1994). The training process means finding appropriate values for the connection weights between the neurons. The relation between the input, the hidden, and the output layers are established by weights "w" and biases "b". The mathematical function, called activation function, has a variety of forms, including hyperbolic tangent, sigmoid, linear, and Gaussian functions. All of these functions are continuous and differentiable. Various learning algorithms such as the combined conjugate gradient, back propagation algorithm, the reducing gradient algorithm, the Bayesian regulating algorithm, and Levenberg-Marquardt algorithm are used for training MLP models. The selection of the algorithm type affects the learning speed and the accuracy of the results (Du et al., 2006; Hassoun and Menhaj, 1994).

Radial based functions (RBF) network which were introduced by Brodhead and Lowe in 1998 for the first time is a type of forward networks with a hidden layer. With sufficient numbers of neurons in the

hidden layer, they are very strong networks in approximation and able to simulate any continuous function with an acceptable degree of accuracy. With some advantages in comparison with the other artificial neural networks, including a better approximation ability, a shorter learning time, a simpler network structure, and avoiding local minimums, the RBF models are used as a reliable tool to simulate various chemical engineering processes (Vaziri and Shahsavand, 2013). This network is composed of three layers. Each layer consists of a number of nodes (neurons), and the nodes in the input layer are used only to pass the input data to the hidden layer; in fact, no calculations are performed in the input layer nodes. Each neuron in the hidden layer has two sets of parameters, namely the center parameter (C_j) and the width or spread parameter (σ_j) associated with it. The activation function of the hidden layer is Gaussian function, and that of the output layer is a linear function. For details in this context can be found elsewhere (Dabiri et al., 2018; Mohebian et al., 2017). All of the data were normalized in the range of 1 to -1. For this purpose, Equation 2 is used:

$$X_{Norm} = 2\left(\frac{X - X_{\text{Min}}}{X_{Max} - X_{Min}}\right) - 1 \tag{2}$$

where, X_{Norm} is normalized data, and X_{Max} and X_{Min} are the maximum and minimum data in the dataset respectively. There are various performance characterization criteria for evaluating the performance of regression techniques. The criteria used for this purpose include the square of the correlation coefficient "R^2", root mean square error "RMSE", and the percentage of average absolute relative error "AARE". Their mathematical definition are given in Equations 3 to 5 (Gandhi and Joshi, 2010; Lashkarbolooki et al., 2012; Alves et al., 2012).

$$R^2 = \frac{\sum_{i=1}^{N}\left(Y_i^{Exp} - \bar{Y}\right)^2 - \sum_{i=1}^{N}\left(Y_i^{Exp} - Y_i^{ANN}\right)^2}{\sum_{i=1}^{N}\left(Y_i^{Exp} - \bar{Y}\right)^2} \tag{3}$$

$$RMSE = \sqrt{\frac{\sum_{i=1}^{N}\left(Y_i^{Exp} - Y_i^{ANN}\right)^2}{N}} \tag{4}$$

$$AARE(\%) = \frac{\sum_{i=1}^{N}\left|\frac{\left(Y_i^{Exp} - Y_i^{ANN}\right)}{Y_i^{Exp}}\right|}{N} \times 100 \tag{5}$$

where, Y_i^{Exp}, $\bar{Y}$, Y_i^{ANN}, and *N* are the experimental values, the average of the experimental values, the artificial neural network output, and the number of samples respectively.

4. Results and discussion

4.1. MLP model structure

Different learning algorithms, including combined conjugate gradient algorithm (Traincgb), the Bayesian algorithm (Trainrp), the reduced gradient algorithm (Traingda), the Broyden-Fletcher-Goldfarb-Shanno (BFGS) algorithm (Trainbfg), and Levenberg-Marquardt algorithm (Trainlm) have been used for training MLP models. In order to determine the most appropriate learning algorithm, 93

data set of the toluene-water system was used in the learning of MLP network. For this purpose, a network with one hidden layer and 8 neurons in the hidden layer was considered so that the ability of the different algorithms is checked. The results of different algorithms for the MLP model are shown in Figure 2.

According to Figure 2, the best algorithm for the simulation is Levenberg-Marquardt. Various structures with different numbers of layers and neurons were studied using the Levenberg-Marquardt algorithm to select the optimized structure of the network. The results of RSME and AARE evaluations are illustrated in Figures 3 and 4 for the various structures of the MLP model applied to the toluene-water system. It is noteworthy that the same investigations were also conducted on the n-butyl acetate-water. According to the evaluation criteria, the best structure for the toluene-water system includes a network with one hidden layer and 8 neurons in the hidden layer. Moreover, the best structure for the n-butyl acetate-water system is a network with one hidden layer and 6 neurons in the hidden layer.

During the calculations, the learning coefficient, the maximum number of iterations, and the momentum factor were determined as 0.01, 10000, and 0.001 respectively. Sigmoid function (tansig) was used as the activation function for all the neurons in the hidden layer. Furthermore, the linear function (purelin) was used for the output layer. The structure of the MLP model of the toluene-water system depicted in Figure 5 includes the input and output layers as well as the number of the hidden layers and neurons in the hidden layer for the network. The experimental data taken from the Kühni extraction column were divided into three distinct sets, including training, validation, and test data. From the total collection of the experimental data, 70% (65 datasets) were used for the training, 15% (14 datasets) for the validation, and 15% (14 datasets) for testing the data.

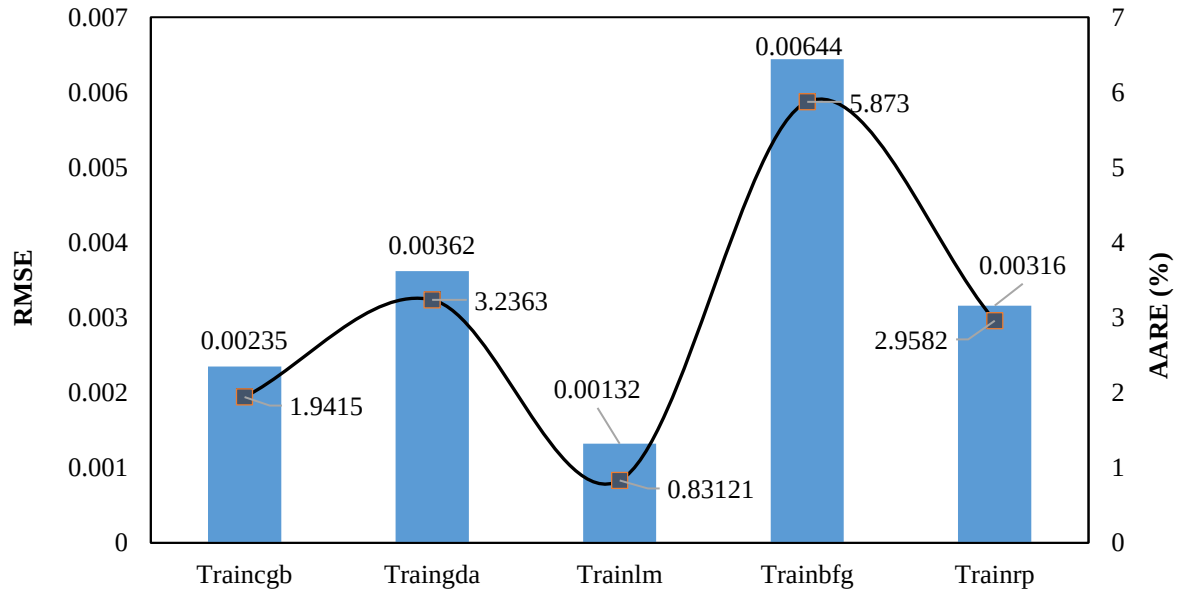

Figure 2

Evaluation criteria of different algorithms in the MLP model.

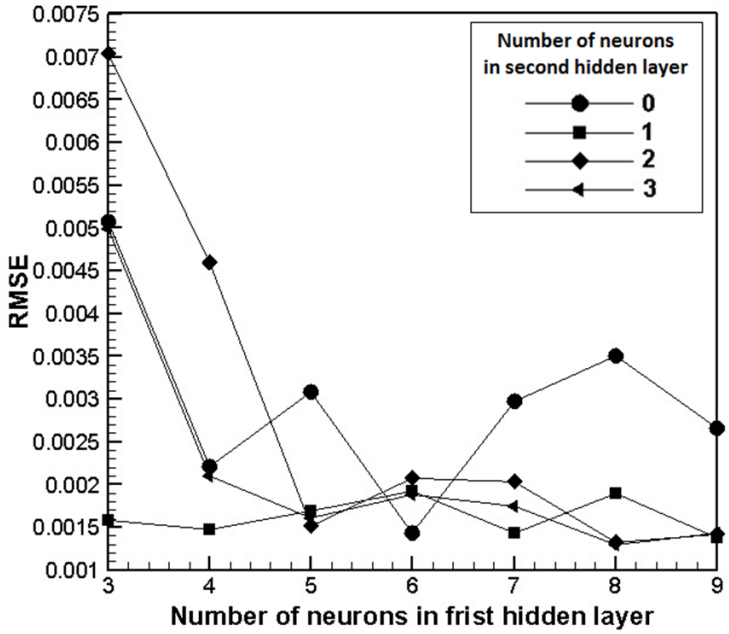

Figure 3

RMSE values of the toluene-water system in the MLP model for structures with different numbers of neurons in the first and the second layers.

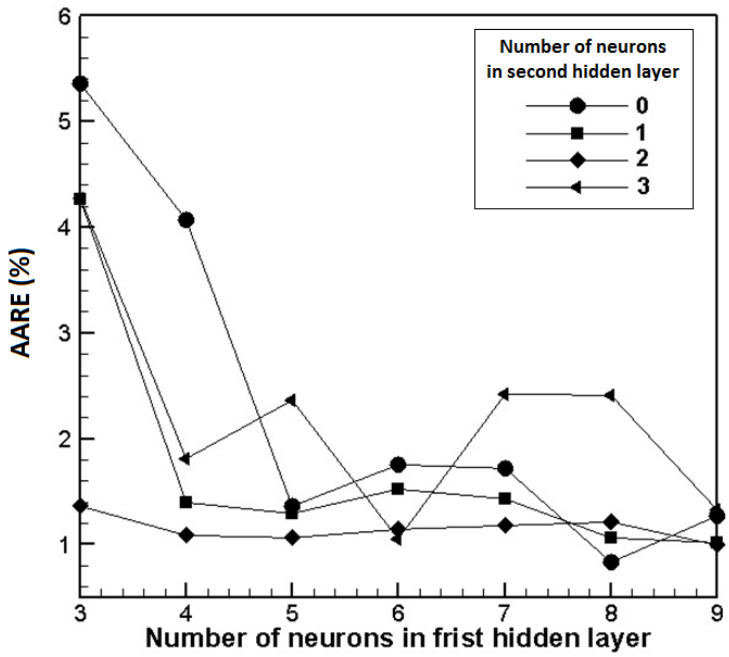

Figure 4

AARE values of the toluene-water system in the MLP model for structures with different numbers of neurons in the first and the second layers.

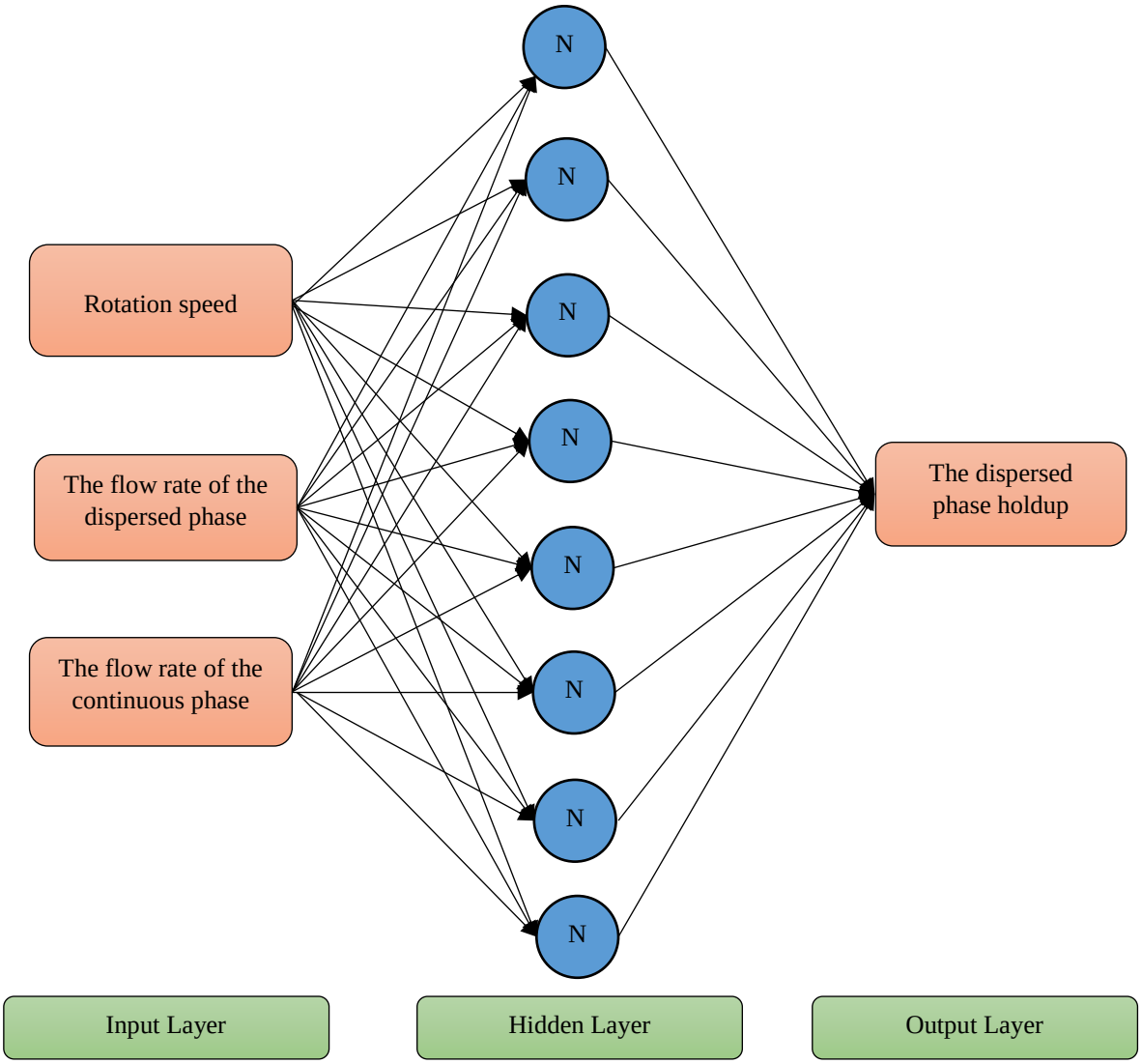

Figure 5

The MLP model structure of the toluene-water system with 8 neurons in one hidden layer.

The values of AARE, RMSE, and R^2 for the network of the toluene-water system were 0.8312, 0.0013, and 0.9990 respectively, and the corresponding values of the n-butyl acetate-water system were 0.8835, 0.0013, and 0.9980 respectively. The comparison between the experimental data and the MLP model predictions for the toluene-water system is given in Figure 6. Figure 6a shows the distribution of all the data and the comparison between the actual and the predicted values, and Figure 6b reveals the extent of the deviations of the data from the model predictions for various amounts of the dispersed phase values; acceptable predictions are obtained by the MLP model. Figure 6c displays the values of errors in various experiments. As shown in this figure, the 38^{th} sample has the maximum error equal to 0.0074. Figure 6d also delineates the frequency distribution of errors.

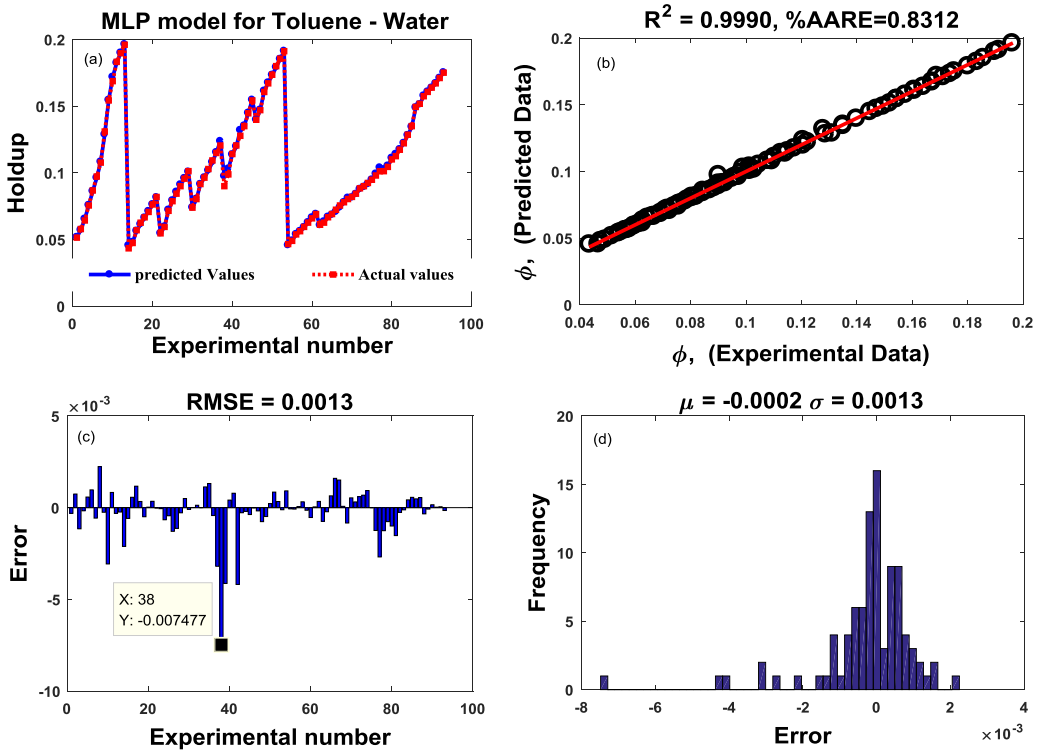

Figure 6

The values predicted by the MLP model against the experimental data for the dispersed phase holdup of the toluene-water system.

4.2. RBF model structure

Gaussian function is used to design the RBF network. The important issue of the RBF model is the spread parameter which plays an important role in improving the generalizability of the network, and it is better to select a large value for it. The magnitude of this parameter depends on the type of problem, and it must be chosen carefully. In addition, the number of neurons must not exceed the half of the number of the training data (Vaziri et al., 2013). A trial and error procedure is used to determine the appropriate number of neurons as well as the spread parameter. Figure 7 displays the variations of RMSE and AARE of the toluene-water system versus the spread parameter and the number of neurons. As can be seen, the lowest values of RMSE and AARE are related to the network with 25 neurons in the middle layer and a spread parameter equal to 22.5.

a)

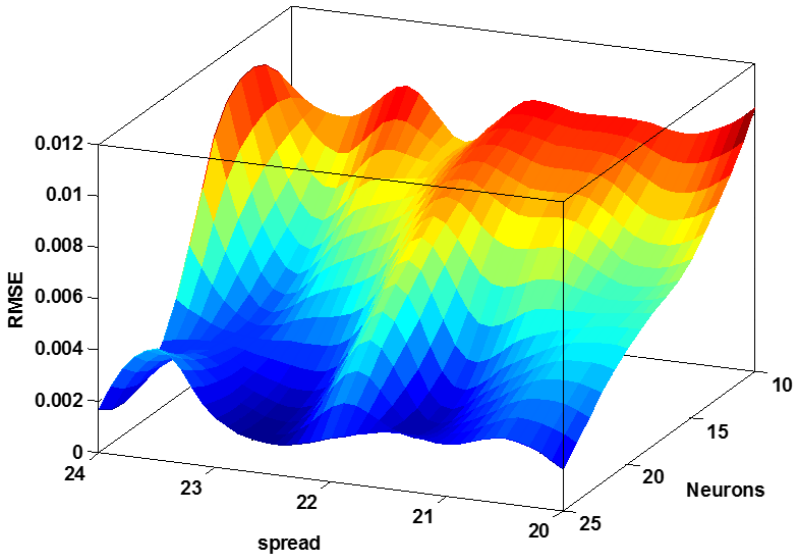

b)

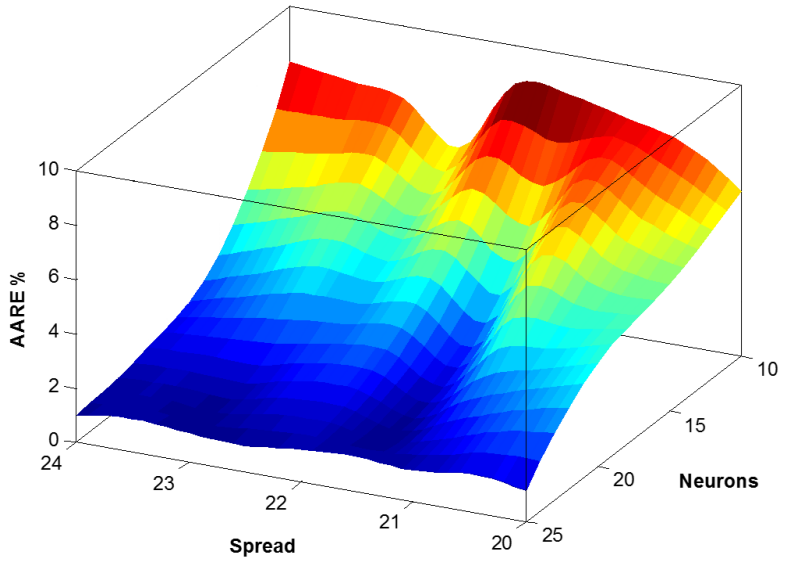

Figure 7

Evaluation results of the toluene-water system based on the spread parameter and the number of neurons in the RBF model: a) RMSE and b) AARE; Minimum AARE and RMSE are 0.97948 and 0.00116 respectively.

In the same manner, a network with 22 neurons in the middle layer and a spread parameter of 19 was determined as the best fitted RBF network for the n-butyl acetate-water system. The evaluation criteria values of AARE, RMSE, and R^2 for the RBF network adapted for the toluene-water system were 0.9795, 0.0012, and 0.9992 respectively, and the corresponding values for the RBF network adapted for the n-butyl acetate-water system were 0.8082, 0.0012, and 0.9987 respectively.

The overall values of the evaluation criteria of the two types of models and the individual evaluations of the training, validation, and testing data are given in Tables 6 and 7; generally, the RBF method represents the best results of the MLP model.

Table 6

Comparison between the evaluation criteria of the toluene-water system.

Evaluation criteria	Data sets	MLP model	RBF model
R^2	Training	0.9997	0.9993
	Validation	0.9970	0.9992
	Test	0.9986	0.9990
	Overall data	0.9990	0.9992
RMSE	Training	0.0006	0.0012
	Validation	0.0026	0.0013
	Test	0.0016	0.0012
	Overall data	0.0013	0.0012
AARE(%)	Training	0.5421	0.8902
	Validation	1.6527	1.1980
	Test	1.3518	1.1755
	Overall data	0.8312	0.9795

Table 7

Comparison between the evaluation criteria of the n-butyl acetate-water system.

Evaluation criteria	Data sets	MLP model	RBF model
R^2	Training	0.9993	0.9994
	Validation	0.9968	0.9980
	Test	0.9989	0.9971
	Overall data	0.9985	0.9987
RMSE	Training	0.0008	0.0008
	Validation	0.0025	0.0014
	Test	0.0012	0.0021
	Overall data	0.0013	0.0012
AARE (%)	Training	0.6583	0.5867
	Validation	2.0406	0.9089
	Test	0.7963	1.7592
	Overall data	0.8835	0.8082

4.3. Effect of operating parameters

The effect of rotor speed on the dispersed phase holdup of both systems is presented in Figure 9. At constant flow rates of the dispersed and continuous phases, the dispersed phase holdup increases by raising the rotor speed of both systems. It is clear that all of the models used for simulating the data of Kühni extractor are excellent in fitting the experimental data. Actually, the droplet breakage increases but droplet size decreases with an increase in rotor speed, which results in an increase in shear forces affecting the droplets. As a result of reducing the droplet size, the relative velocity between the continuous phase and the dispersed phase (slip velocity) falls, and the dispersed phase holdup rises with an increase in the number of the droplets within the column.

A comparison between the curves in Figure 8 confirms that an increase in the interfacial tension leads to a drop in the dispersed phase holdup. That is, the dispersed phase holdup of the toluene-water system, with a higher interfacial tension, is less than that of the n-butyl acetate-water system. In fact, increasing interfacial tension raises the droplet size and consequently the slip velocity between the phases. A reduction in the residence time of the droplets corresponds to a drop in the dispersed phase holdup. By using the output predictions from the intelligent methods, one can detect the effect of rotor speed on the variations of the dispersed phase holdup at rotor speeds beyond the range of the data.

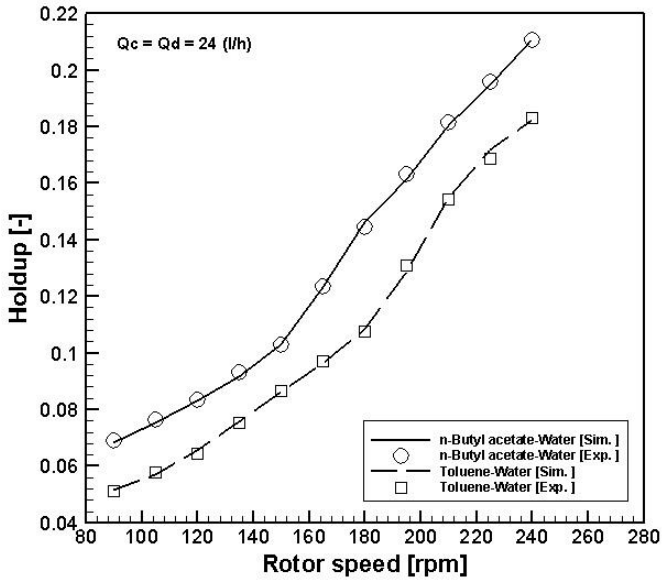

Figure 8

Effect of rotor speed on the dispersed phase holdup.

The effect of the flow rate of the dispersed phase on the dispersed phase holdup of both systems is depicted in Figures 9 and 10. The number and frequency of droplet coalescence increase at an increased flow rate of the dispersed phase, when the rotor speed and the flow rate of the continuous phase are kept constant. Thus, the dispersed phase holdup rises at a higher number of drops. Figure 11 depicts the effects of rotor speed and the flow rate of the dispersed phase on the dispersed phase holdup at two different constant flow rates of the continuous phase. As can be inferred from this figure, raising the flow rate of the dispersed phase at all values of the rotor speed and at the flow rates of the continues phase equal to 30 and 60 (l/hr.) improves the dispersed phase holdup of the toluene-water system.

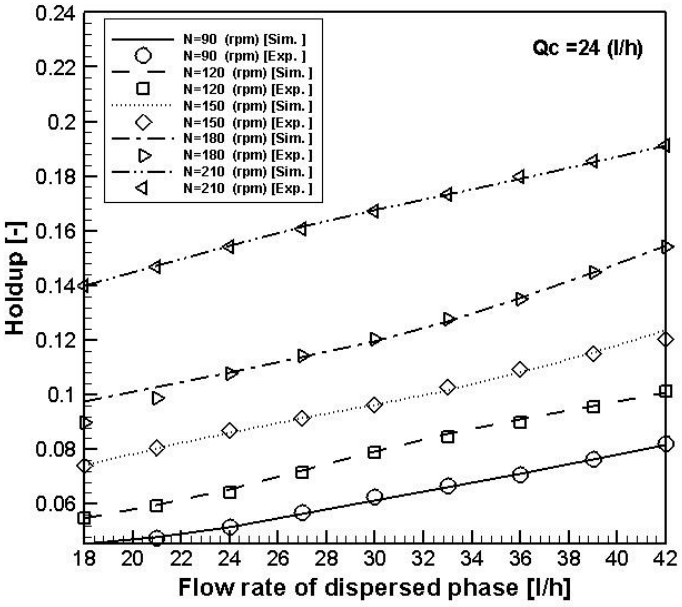

Figure 9

Effect of the flow rate of the dispersed phase on the dispersed phase holdup of the toluene-water system.

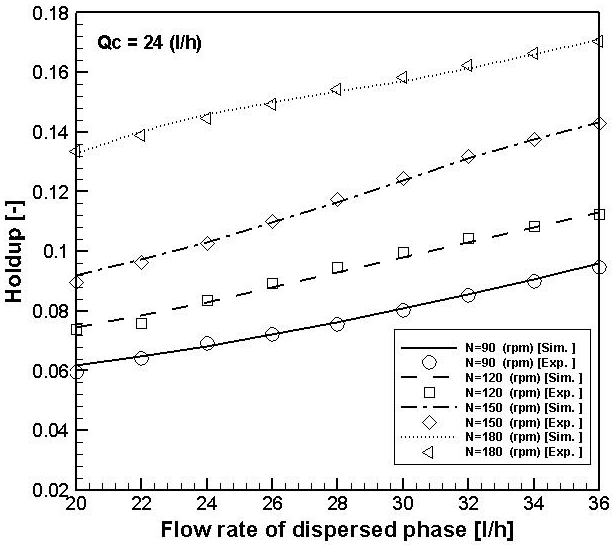

Figure 10

Effect of the flow rate of the dispersed phase on the dispersed phase holdup of the n-butyl acetate-water system.

a)

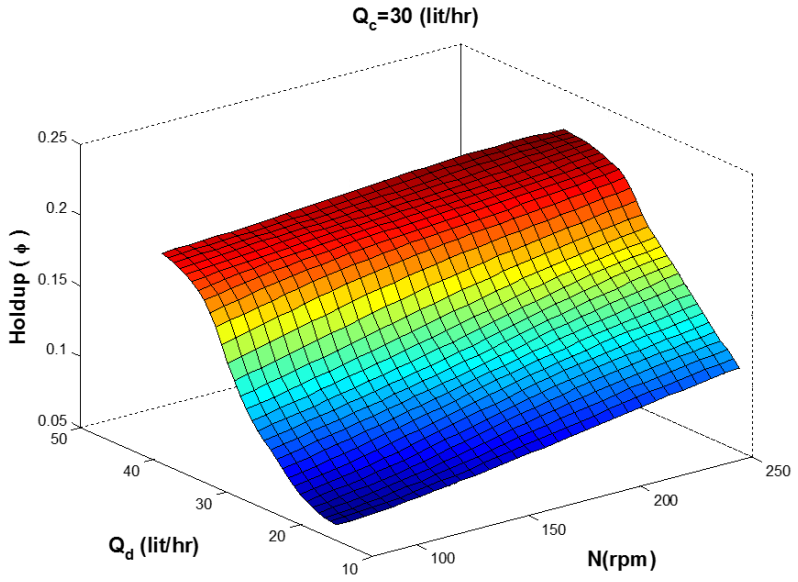

b)

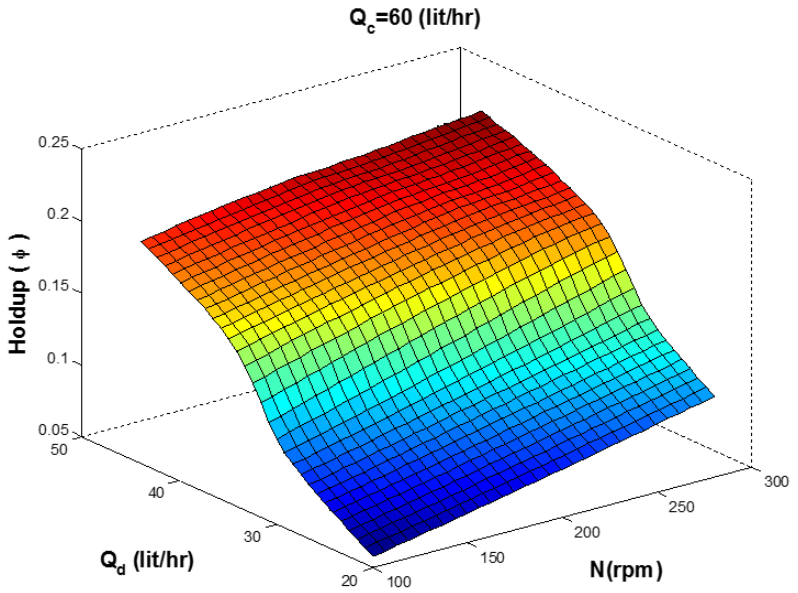

Figure 11

Variations of the dispersed phase holdup versus the rotor speed and the flow rate of the dispersed phase of the toluene-water system: a) $Q_c = 30$ ($\frac{\text{lit}}{\text{hr.}}$) and b) $Q_c = 60$ ($\frac{lit}{hr.}$).

Figures 12 and 13 illustrate the effect of the flow rate of the continuous phase on the dispersed phase holdup. Increasing the flow rate of the continuous phase at a constant rotor speed and a constant flow rate of the dispersed phase raises the drag force between the continuous phase and the dispersed phase, which results in limitation to the droplet movement and consequentially enhances the dispersed phase holdup. Comparing Figures 9 and 10 with Figures 12 and 13 states that the effect of flow rate of the dispersed phase on the dispersed phase holdup is larger than that of the continuous phase in both systems.

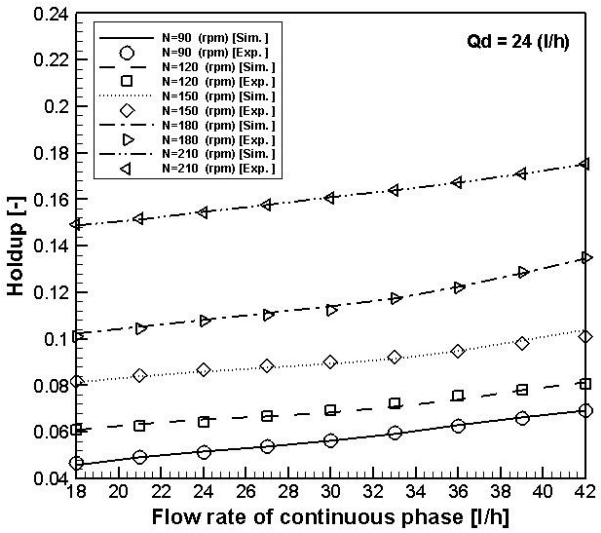

Figure 12

Effect of the flow rate of the continuous phase on the dispersed phase holdup of the toluene-water system.

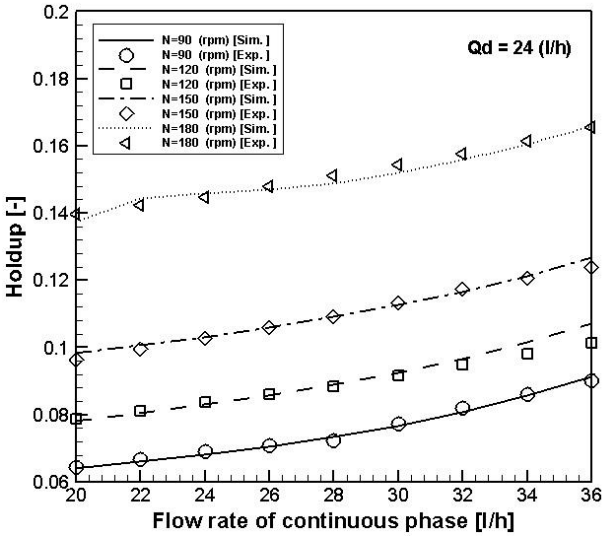

Figure 13

Effect of the flow rate of the continuous phase on the dispersed phase holdup of the n-butyl acetate-water system.

One of the objectives of this work is comparing the ability of different modeling methods and empirical correlations to predict the dispersed phase holdup. To this end, a set of 174 experimental data (93 data sets for the toluene-water system and 81 data sets for the n-butyl acetate-water system) are used. 150 data sets are used to produce the intelligent networks, and the remaining 24 data sets are employed to determine the empirical correlation coefficients and thus compare the performance of the models. The dispersed phase holdup is correlated with the operational conditions and the physical properties of the systems by the 150 datasets as follows:

$$\phi = 0.4763\left(\frac{g\gamma}{\rho_c V_d^4}\right)^{-0.9890}\left(\frac{\mu_d}{\mu_c}\right)^{0.1095}\left(\frac{N\gamma}{V_d^3\rho_c}\right)^{1.1265}\left(\frac{\Delta\rho}{\rho_c}\right)^{-1.6421}\left(\frac{V_c}{V_d}\right)^{0.2035} \quad (6)$$

where, ϕ, g, γ, ρ_c, V_d, V_c, μ_d, μ_c, N, and $\Delta\rho$ are the dispersed phase holdup, gravitational force, interfacial tension, the continuous phase density, the dispersed phase velocity, the continuous phase

velocity, the dispersed phase viscosity, the continuous phase viscosity, rotation speed, and the density difference between the phases respectively. In Equation 6, the evaluation criteria of AARE, RMSE, and R^2 for fitting the data are 6.6132, 0.0098, and 0.9653 respectively. Figure 14 compares the ability of the intelligent models and that of the correlation in Equation 6 to predict the dispersed phase holdup. It also reveals that the RBF model performs better than the MLP and empirical correlation in predicting the new data sets. According to Equation 5, the absolute percentage error of the empirical correlations, MLP network, and RBF network are 4.332%, 2.642%, and 2.192% respectively.

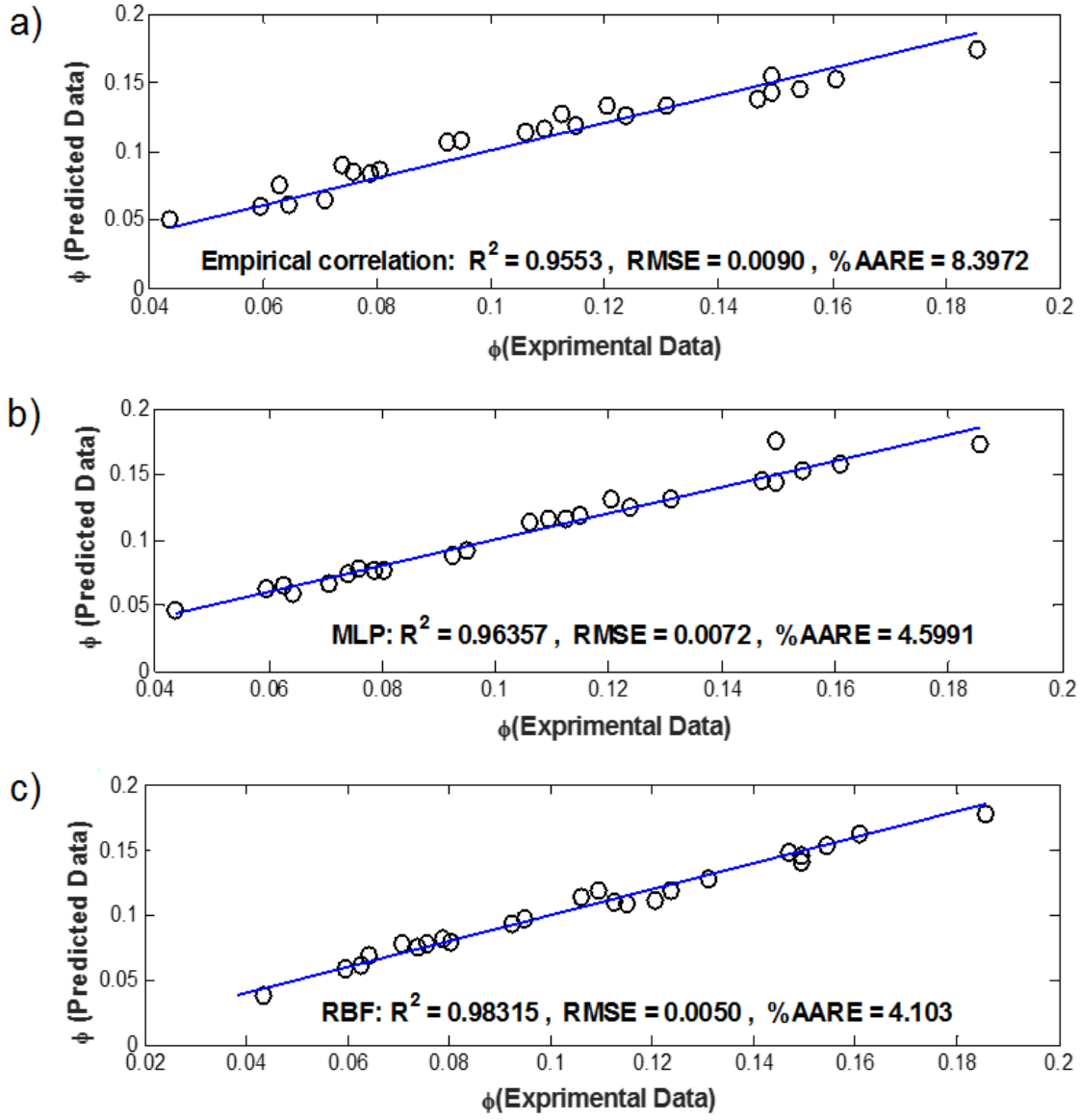

Figure 14

The actual and predicted dispersed phase holdup for 24 intact datasets: a) empirical correlations, b) MLP, and c) RBF.

5. Conclusions

In this research, the experimental investigation and simulation of the dispersed phase holdup are considered in a Kühni column. In the simulation, using intelligent techniques, a method is provided which reduces the need for the experimental data. For this purpose, two contacting systems of toluene-water and n-butyl acetate-water are investigated. The intelligent models, including MLP and RBF

models are used in an optimal structure to simulate the dispersed phase holdup. Additionally, an empirical correlation is employed to predict the dispersed phase holdup as a function of the physical properties and the operation variables. Finally, the following results are obtained:

- The dispersed phase holdup increases at higher rotor speeds at a constant flow rate of the dispersed and continuous phases.
- The interfacial tension has a significant impact on the dispersed phase holdup. An increase in the interfacial tension expands the droplets, which results in a higher relative phase velocity; consequently, the dispersed phase holdup drops.
- Increasing the flow rate of the dispersed phase at a constant rotor speed and a constant flow rate of the continuous phase enhances the dispersed phase holdup.
- By increasing the flow rate of the continuous phase at a constant rotor speed and a constant flow rate of the dispersed phase, the drag force for moving the droplets rises and the speed of the droplets climbing up falls, resulting in an increase in the dispersed phase holdup.
- Among the operation parameters, the rotor speed has the greatest impact on the dispersed phase holdup.
- Among the three different modeling techniques applied to the data of Kühni extraction column, including MPL, RBF, and the empirical correlating method, the RBF modeling is proved to most accurately fit the data of the systems.
- The ability of the artificial neural network to predict anonymous data can be used to reduce the number of the relevant experiments and to lower the cost of the experiments; therefore, with fewer experiments, the desired result is achieved. In order to improve the results and predictions, using machine learning methods (support vector regression) and comparing them with ANN methods are suggested.

Nomenclature

AARE	Average absolute relative error (%)
D	Column diameter (m)
D_s	Stator opening diameter (m)
g	Acceleration duo to gravity (m/s^2)
h_c	Compartment height (m)
N	Rotor speed (1/s)
Q	Flow rate of the dispersed or continuous phases (m^3/s)
R	Correlation coefficient (-)
RMSE	Root mean square error (-)
V	Superficial velocity (m/s)
V_s	Slip velocity (m/s)
W	Weight factor (-)
x_i	Input examples (attributes)
y_i	Target output
Greek letters	
$\Delta\rho$	Density difference between the phases (kg/m^3)

ϕ	Dispersed phase holdup (-)
ψ	Mechanical power dissipation per unit mass (w/kg)
γ	Interfacial tension (N/m)
μ	Viscosity (Pa.s)
ρ	Density (kg/m^3)
σ	Width of radial basis function (RBF) kernel (-)
Subscripts	
c	Continuous phase
d	Dispersed phase
j	Number of neurons in hidden layer
Superscripts	
T	Transpose

Reference

Alves J. C. L., Henriques C. B., and Poppi R. J., Determination of Diesel Quality Parameters Using Support Vector Regression and Near Infrared Spectroscopy for an In-line Blending Optimizer System, Fuel, Vol. 97, p. 710–717, 2012.

Arab E., Ghaemi A., and Torab-Mostaedi M., Experimental Investigation of Slip Velocity and Dispersed Phase Holdup in a Kühni Extraction Column, Asia-Pacific Journal of Chemical Engineering, Vol. 12, p. 620–630, 2017.

Asadollahzadeh M., Shahhosseini S., Torab-Mostaedi M., and Ghaemi A., Mass Transfer Performance in an Oldshue–Rushton Column Extractor, Chemical Engineering. Research Design, Vol. 100, p. 104–112, 2015b.

Asadollahzadeh M., Torab-Mostaedi M., Shahhosseini S., and Ghaemi A., Using Maximum Entropy Approach for Prediction of Drop Size Distribution in a Pilot Plant Multi-impeller Extraction Contactor, RSC Advances, Vol. 5, p. 95967–95980, 2015a.

Attarakih M., Hlawitschka M. W., Abu-Khader M., Al-Zyod S., and Bart H.-J., CFD-population Balance Modeling and Simulation of Coupled Hydrodynamics and Mass Transfer in Liquid Extraction Columns, Applied Mathematical Model, Vol. 39, p. 5105–5120, 2015.

Broomhead D. S. and Lowe D., Radial Basis Functions, Multi-variable Functional Interpolation and Adaptive Networks, Royal Signals and Radar Establishment Malvern (United Kingdom), 1988.

Buchbender F., Onink F., Meindersma G. W., and Pfennig A., Simulation of Aromatics Extraction with an Ionic Liquid in a Pilot-plant Kühni Extractor Based on Single-drop Experiments, Chemical Engineering Science, Vol. 82, p. 167–176, 2012.

Chen J., Fu R., Xu S., Wu Q., and Song C., Measurement of Interface Level, Holdup, Pulsation Frequency, and Amplitude in a Pulsed Column by Air Purge, Industrial Engineering and Chemical Research, Vol. 41, No. 7, p. 1868–1872, 2002.

Dabiri-atashbeyk M., Koolivand-Salooki M., and Esfandyari M., Comparing Two Methods of Neural Networks to Evaluate Dead Oil Viscosity, Iranian Journal of Oil & Gas Science and Technology, Vol. 7, p. 60–69, 2018.

Du K.L. and Swamy M. N. S., Neural Networks in a Soft-computing Framework, Springer Science & Business Media, 2006.

Gandhi A. B., Joshi J. B., Estimation of Heat Transfer Coefficient in Bubble Column Reactors Using Support Vector Regression, Chemical Engineering Journal, Vol. 160, p. 302–310, 2010.

Gomes L. N., Guimarães M. L., Regueiras P. F. R., Stichlmair J., and Cruz Pinto J. J., Simulated and Experimental Dispersed-phase Breakage and Coalescence Behavior in a Kühni Liquid-liquid Extraction Column Steady State, Industrial Engineering Chemical Research, Vol. 45, p. 3955–3968, 2006.

Hagan M. T. and Menhaj M. B., Training Feedforward Networks with the Marquardt Algorithm, Neural Networks, IEEE Transaction, Vol. 5, p. 989–993, 1994.

Hassoun M. H., Fundamentals of Artificial Neural Networks, Proceedings of IEEE, 84, 1996.

Haunold C., Cabassud M., Gourdon C., and Casamatta G., Drop Behavior in a Kühni Column for a Low Interfacial Tension System, Canadian Journal of Chemical Engineering, Vol. 68, p. 407–414, 1990.

Hemmati A. R., Shirvani M., Torab-Mostaedi M., and Ghaemi A., Hold-up and Flooding Characteristics in a Perforated Rotating Disc Contactor (PRDC), RSC Advances, Vol. 5, p. 63025–63033, 2015.

Hemmati A. R., Torab-Mostaedi M., Shirvani M., and Ghaemi A., A Study of Drop Size Distribution and Mean Drop Size in a Perforated Rotating Disc Contactor (PRDC), Chemical Engineering Research and Design, Vol. 96, p. 54–62, 2015.

Hufnagl H., McIntyre M., and Blaß E., Dynamic Behavior and Simulation of a Liquid-liquid Extraction Column, Chemical Engineering and Technology, Vol. 14, p. 301–306, 1991.

Kumar A. and Hartland S., A Unified Correlation for the Prediction of Dispersed-phase Holdup in Liquid-liquid Extraction Columns, Industrial Engineering Chemical Process Design Development, Vol. 34, p. 3925–3940, 1995.

Lashkarbolooki M., Shafipour Z. S., and Hezave A. Z., Trainable Cascade-forward Back-propagation Network Modeling of Spearmint Oil Extraction in a Packed Bed Using SC-CO_2, Journal of Supercritical Fluids, Vol. 73, p. 108–115, 2013.

Mohebian R., Riahi M. A., and Kadkhodaie-Ilkhchi A., A Comparative Study of the Neural Network , Fuzzy Logic, and Nero-fuzzy Systems in Seismic Reservoir Characterization: An Example from Arab (Surmeh) Reservoir as an Iranian Gas Field, Persian Gulf Basin, Iranian Journal of Oil & Gas Science and Technology, Vol. 6, p. 33–50, 2017.

Moreira É., Pimenta L. M., Carneiro L. L., Faria R. C. L., Mansur M. B., and Cláudio J. R. P., Hydrodynamic Behavior of a Rotating Disc Contactor under Low Agitation Conditions, Chemical Engineering Communication, Vol. 192, No. 8, p. 1017–1035, 2005.

Mögli A. and Bühlmann U., The Kühni Extraction Column, Handbook of Solvent Extraction, Wiley, New York, 1983.

Neto A. P. and Mansur M. B., Transient Modeling of Zinc Extraction with D2EHPA in a Kühni Column, Chemical Engineering Research and Design, Vol. 91, p. 2323–2332, 2013.

Oliveira N. S., Silva D. M., Gondim M. P. C., and Mansur M. B., A Study of the Drop Size Distributions and Holdup in Short Kühni Columns, Brazilian Journal of Chemical Engineering, Vol. 25, p. 729–741, 2008.

Rode S., Durand A., Mabille I., and Favre E., Flooding Characteristics of an Aqueous Two-phase System in a Counter-current Kühni-type Column, Chemical Engineering Science, Vol. 98, p. 98–103, Jul. 2013.

Rumelhart D. E., Hinton G. E., and Williams R. J., Learning Representations by Back-propagating Errors, Nature, Vol. 323, p. 533, 1986.

Sharker S., Phillips C. R., and Mumford C. J., Characterization of Hydrodynamic Parameters in Rotating Disc and Oldshue-Rushton Columns: Hydrodynamic Modelling, Drop Size, Hold-up and Flooding, Canadian Journal of Chemical Engineering, Vol. 63, p. 701–709, 1985.

Tahershamsi A. H., Ghaemi A., and Shirvani M., Modeling and Simulation of Kühni Extraction Column Using a Rate-based Model, Iranian Journal of Oil & Gas Science and Technology, Vol. 5, p. 53–67, 2016.

Torab-Mostaedi M., Ghaemi A., Asadollahzadeh M., and Pejmanzad P., Mass Transfer Performance in Pulsed Disc and Doughnut Extraction Columns, Brazilian Journal of Chemical Engineering, Vol. 28, p. 447–456, 2011.

Torab-Mostaedi M., Jalilvand H., and Outokesh M., Dispersed Phase Holdup in a Pulsed Disc and Doughnut Extraction Column, Brazilian Journal of Chemical Engineering, Vol. 28, p. 313–323, 2011.

Vaziri B. M. and Shahsavand A., Analysis of Supersonic Separators Geometry Using Generalized Radial Basis Function (GRBF) Artificial Neural Networks, Journal of Natural Gas Science Engineering, Vol. 13, p. 30–41, 2013.